（ ※本報告書は英語で記述してください。ただし、産業利用課題として採択されている方は日本語で記述していただいても結構です。 ）

| CROSS TOKAI **Experimental Report** J-PARC | 承認日 Date of Approval 5/8, 2017<br>承認者 Approver HARJO Stefanus<br>提出日 Date of Report 4/24, 2017 |
|---|---|
| 課題番号 Project No.<br>2016E0003<br>実験課題名 Title of experiment<br>In-situ Neutron Diffraction Analysis for Deformation and Phase Transformation Behaviors of Advanced Structural Metallic Materials<br>実験責任者名 Name of principal investigator<br>Nobuhiro Tsuji<br>所属 Affiliation<br>Kyoto University | 装置責任者 Name of Instrument scientist<br>BL19 Kazuya Aizawa<br>装置名 Name of Instrument/(BL No.)<br>BL19<br>実施日 Date of Experiment<br>(1) 11/25-11/26, 2016<br>(2) 2/17-2/18, 2017 |

試料、実験方法、利用の結果得られた主なデータ、考察、結論等を、記述して下さい。（適宜、図表添付のこと）
Please report your samples, experimental method and results, discussion and conclusions. Please add figures and tables for better explanation.

1. 試料 Name of sample(s) and chemical formula, or compositions including physical form.

(1) 11/25-11/26, 2016

Fe-2Mn-0.1C, Fe-24Ni-0.3C, Fe-18Cr-8Ni, pure Mg

(2) 2/17-2/18, 2017

Fe-5Mn-2Si-0.1C, Fe-2Mn-0.1C, Fe-2Mn-0.4C, Fe-10Ni-0.1C, Ti-6Al-4V

2. 実験方法及び結果（実験がうまくいかなかった場合、その理由を記述してください。）
Experimental method and results. If you failed to conduct experiment as planned, please describe reasons.

**(1) *In-situ* neutron diffraction analysis for peculiar deformation behavior of advanced metallic materials**

As shown in the schematic illustration of **Figure 1**, a tensile test specimen was mounted at the standard tensile testing system at BL19 TAKUMI as that the tensile axis to be aligned 45° with respect to the incident beam. The neutron diffraction profiles in the axial and transverse directions of the specimen during tensile deformation at room temperature were measured simultaneously by using two time-of-flight detector banks that have scattering angle of ±90 °. We studied deformation behaviors of four kinds of materials. The results are summarized as follows.

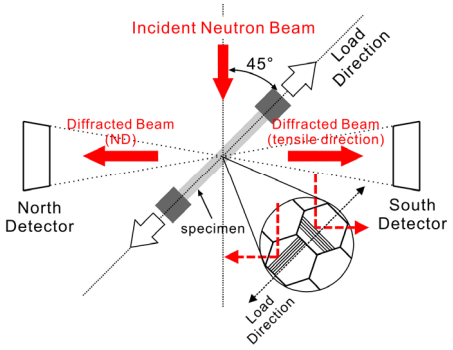


**Figure 1** Schematic illustration showing an alignment of a tensile test specimen with respect to the incident and diffracted neutron beams.

2. 実験方法及び結果（つづき） Experimental method and results (continued)

**(1-1) Deformation behavior of dual phase steel composed of ferrite and martensite**

Dual-Phase (DP) steels composed of a soft ferrite phase and a hard martensite phase are widely used in the industrial field due to their excellent mechanical properties such as high strength, adequate ductility, and good cost performance. To understand the deformation behavior of DP steels is important for further improvement of mechanical properties of DP steels. In the present experiment, we studied deformation behavior of the DP steel (Fe-2Mn-0.1C) with different grain sizes (coarse-grained DP (d = 58.3 μm) and fine-grained DP (d = 4.1 μm)) by *in-situ* neutron diffraction during tensile deformation. **Figure 2** shows lattice elastic strains of ferrite and martensite during tensile deformation at room temperature (the data of the coarse-grained DP were obtained in the former experiment of 2015E0001). The elastic strains of ferrite and martensite phases increase linearly along the line corresponding to Young's modulus when the applied stress is smaller than approximately 200 MPa. After the applied stress increases larger than 200 MPa, elastic strain of martensite phases becomes very large compared with ferrite. In addition, it is clear that martensite of the fine-grained DP exhibits much higher elastic strain than that of the coarse-grained DP. This result indicates that the high strength of the fine-grained DP results from the large elastic strain of martensite.

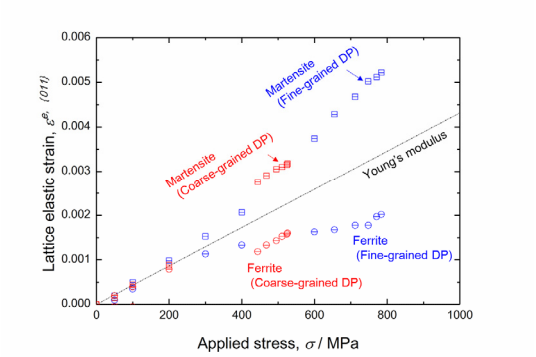


**Figure 2** Lattice elastic strains of ferrite and martensite during tensile deformation in the different grain-sized DP specimens.

**1-2 Deformation behavior of metastable austenitic steel**

Transformation-induced plasticity (TRIP) effect is one of the promising ways to achieve high strength and large ductility simultaneously by utilizing deformation-induced martensitic transformation. However, the underlying mechanism for the superior mechanical property of TRIP effect is still unclear. In the present experiment, deformation behavior of the metastable austenitic steel (Fe-24Ni-0.3C) was studied by *in-situ* neutron diffraction during tensile deformation. **Figure 3** shows work-hardening rate and volume fraction of martensite during tensile deformation. The (111), (200), (220), (311) diffraction peaks of austenite and the (110), (200), (211), (220) diffraction peaks of martensite were used to calculate the volume fraction of martensite. The result suggests that the enhanced work-hardening occurs after the onset of deformation-induced martensitic transformation. **Figure 4** shows the changes in phase stresses of austenite and martensite along the tensile direction.

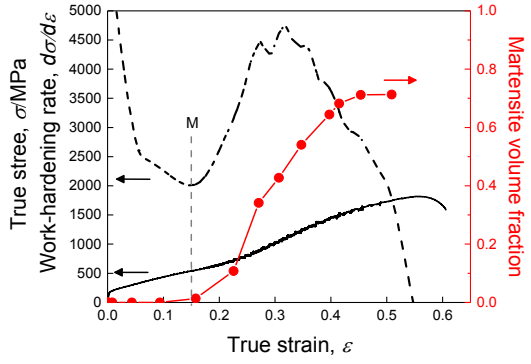


**Figure 3** True stress – true strain curve, work-hardening curve, and the volume fraction of martensite measured by neutron diffraction.

The phase stresses were estimated from the lattice elastic strains of austenite ((111) plane) and martensite ((011) plane). It can be found that the phase stress of martensite significantly increases with increasing tensile strain. In addition, calculated total stress coincides very well with the experimentally obtained stress-strain curve. The stress contribution of martensite and austenite on macroscopic flow stress is summarized in **Figure 5**. With increasing tensile strain, the stress contribution of martensite quickly increases, while that of austenite gradually decreases. Consequently, we can conclude that the enhanced work-hardening is mainly attributed to the phase stress of martensite.

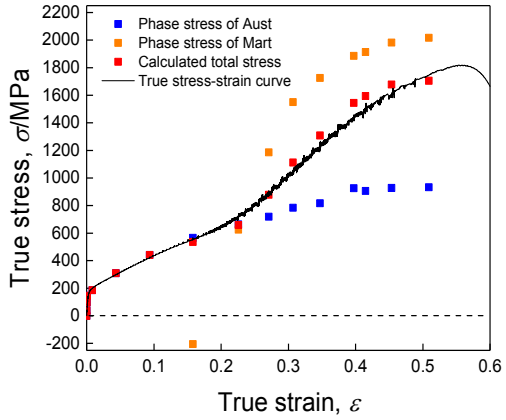


**Figure 4** Phase stresses of austenite and martensite superimposed on the true stress – true strain curve.

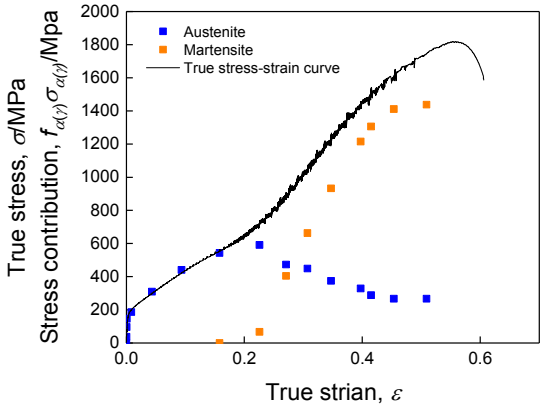


**Figure 5** Stress contributions of martensite and austenite on macroscopic flow stress.

## 1-3 Deformation behavior of ultrafine-grained pure Mg

Three kinds of pure Mg specimens with grain size of 0.65 μm (ultrafine grain, UFG), 2.46 μm (fine grain, FG), and 7.27 μm (coarse grain, CG), respectively, were prepared and deformation behaviors of the pure Mg with various grains sizes were investigated by *in-situ* neutron diffraction during tensile deformation. **Figure 6** shows stress-strain curves of the above three specimens under uniaxial tensile test with an initial strain rate of $8.3\times10^{-4}$ $s^{-1}$. It is very interesting that the UFG specimen shows the lowest yield strength and very large tensile elongation of about 100%. The FG specimen exhibits the highest yield strength and tensile elongation of 26%. The CG specimen shows lower yield strength and comparable tensile elongation compared to the FG specimen. **Figure 7** shows relative full width at half maximum (FWHM) of several typical neutron diffraction peaks as a function of tensile strain in the above three specimens.

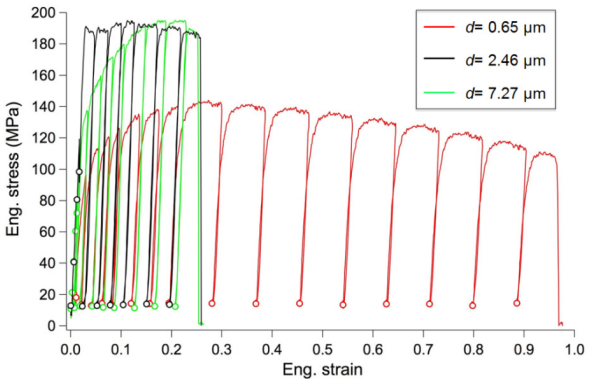


**Figure 6** Stress - strain curves of the specimens with different grain sizes. The open circles indicate the interrupted strains for neutron diffraction measurement.

2. 実験方法及び結果（つづき） Experimental method and results (continued)

The value of the relative FWHM reflects the evolution of dislocation density at various strain levels. For the UFG specimen, the values of relative FWHM remain low (around 1~1.2) at all the interrupted strains, indicating that dislocation slip is not the dominant deformation mode. The large tensile elongation may be associated with the enhanced grain boundary sliding behavior in the UFG specimen, which may also reduce the yield strength. For the FG specimen, the values of relative FWHM increase very quickly with increasing tensile strain, suggesting that dislocation slip is one of the major deformation modes. For the CG specimen, the relative FWHM values also increase significantly with increasing tensile strain. However, the relative FWHM values of the CG specimen are always lower than that of the FG specimen at same strain levels. It has been proposed that deformation twinning, which is another important deformation mode in Mg, is inhibited by grain refinement. Thus, deformation twinning may also play an important role in the CG specimen, which could reduce the number of dislocations that are required for accommodating plastic strain.

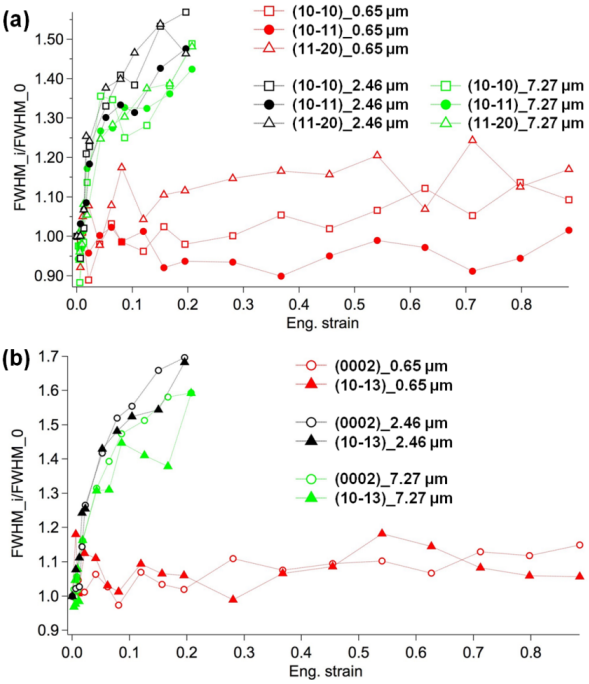


**Figure 7** Relative full width at half maximum (FWHM) of several diffraction peaks as a function of tensile strain. (a) Diffraction peaks along the axial direction, (b) diffraction peaks along the transverse direction.

**1-4 Deformation behavior of ultrafine-grained SUS304 austenitic stainless steel**

SUS304 stainless steel is a widely used commercial stainless steel due to its high corrosion resistance and good workability. However, it has a relatively low yield strength due to the FCC lattice structure. It is expected that ultra-grain refinement is an effective way to increase the yield strength of SUS304 austenitic steel according to the well-known Hall-Petch relationship.

We prepared the SUS304 austenitic steels with different grain sizes from 0.24 to 17.24 μm, and investigated deformation behavior by *in-situ* neutron diffraction during tensile deformation. **Figure 8** shows stress - strain curves of the specimens having different grain sizes during *in-situ* neutron diffraction experiment. It is seen that the deformation behavior is significantly different according to different grain sizes. High strength and good tensile ductility are achieved when the grain size is 0.24 μm. The volume fractions of deformation-induced martensite were measured by integrate the intensity of the diffraction peaks of austenite and martensite. Changes of martensite volume fraction are summarized as a function of tensile strain in **Figure 9**. It is very interesting to note that the refinement of austenite grain enhances the kinetics of deformation-induced martensitic transformation, which is opposite tendency from the previous research results on other austenitic steels. It has been

believed that grain refinement increases the stability of austenite and thus inhibits martensitic transformation. However, the present results suggest that grain refinement greatly accelerates the deformation-induced martensitic transformation.

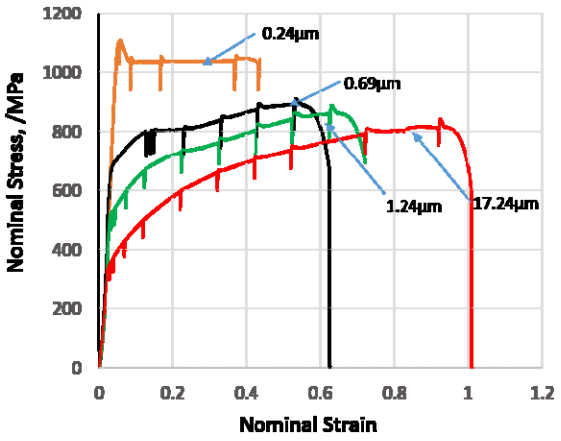


**Figure 8** Stress - strain curves of the specimens with different grain sizes.

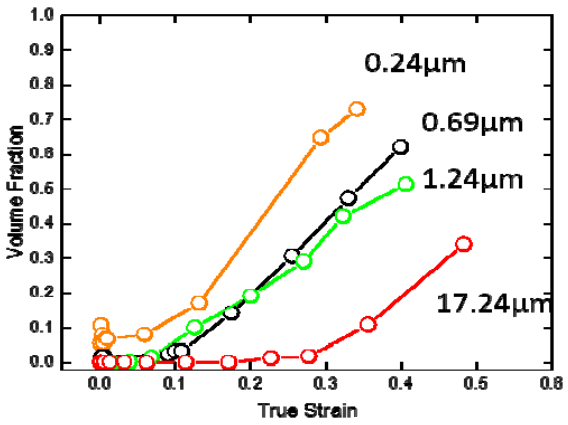


**Figure 9** Changes of martensite volume fraction as a function of strain.

**(2) *In-situ* neutron diffraction analysis for deformation and phase transformation behaviors at elevated temperature**

We used the newly developed thermomechanical processing simulator for *in-situ* neutron diffraction analysis which can be applicable to BL19 TAKUMI in J-PARC / MLF (**Figure 10**). This simulator can heat specimen up to 1200 °C by induction heating system under vacuum condition or gas atmosphere, and can apply precisely controlled compression deformation at a maximum deformation rate of 100 mm $s^{-1}$ with a maximum load of 30 kN. Load and displacement of the compressive deformation are recorded so that we can obtain stress - strain curve of the deformation.

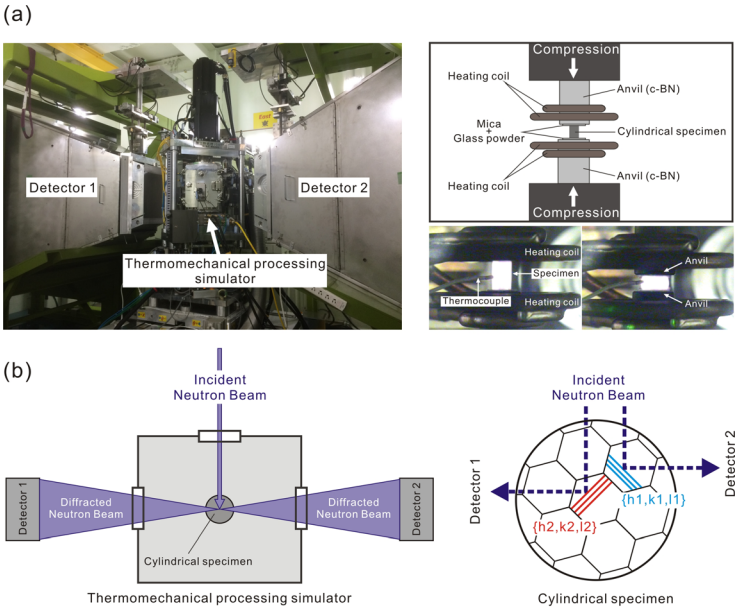


**Figure 10** (a) The thermomechanical processing simulator installed at the BL 19 TAKUMI and schematic illustration of the testing part of the simulator (b) the geometry of the compression experiment with respect to the incident and diffracted neutron beams.

2. 実験方法及び結果（つづき） Experimental method and results (continued)

**(2-1) Phase transformation behavior of medium Mn steel during thermomechanical processing**

Medium Mn steels containing 3 ~ 7 mass % are expected as the new class of advanced high strength steels because of their nice strength-ductility balance. Accordingly, numerous research groups all over the world are competitively studying medium Mn steels now. In order to further improve mechanical properties of medium Mn steels based on theoretical backgrounds, quantitative evaluations of microstructure evolutions during thermomechanical processing are necessary.

In the present study, austenite reverse transformation behaviors of the medium Mn steel (Fe-5Mn-2Si-0.1C) were investigated by *in-situ* neutron diffraction using the newly developed thermomechanical processing simulator. **Figure 11** shows the conducted thermomechanical processing. The volume fractions of reversely transformed austenite at 640 °C, 700 °C, and 720 °C (black plots: without deformation, red plots: with compressive deformation at a strain rate of 1 $s^{-1}$) are presented in **Figure 12**. The results indicate that the deformation greatly accelerates the reverse austenitic transformation. Particularly, the reversely transformed austenite reaches to equilibrium fraction by the deformation at 700 °C and 720 °C.

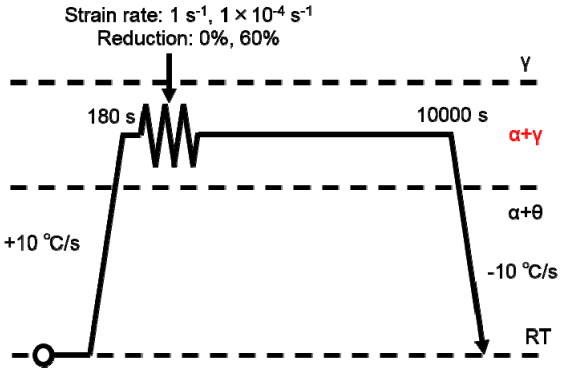


**Figure 11** Schematic illustration showing the conducted thermomechanical processing.

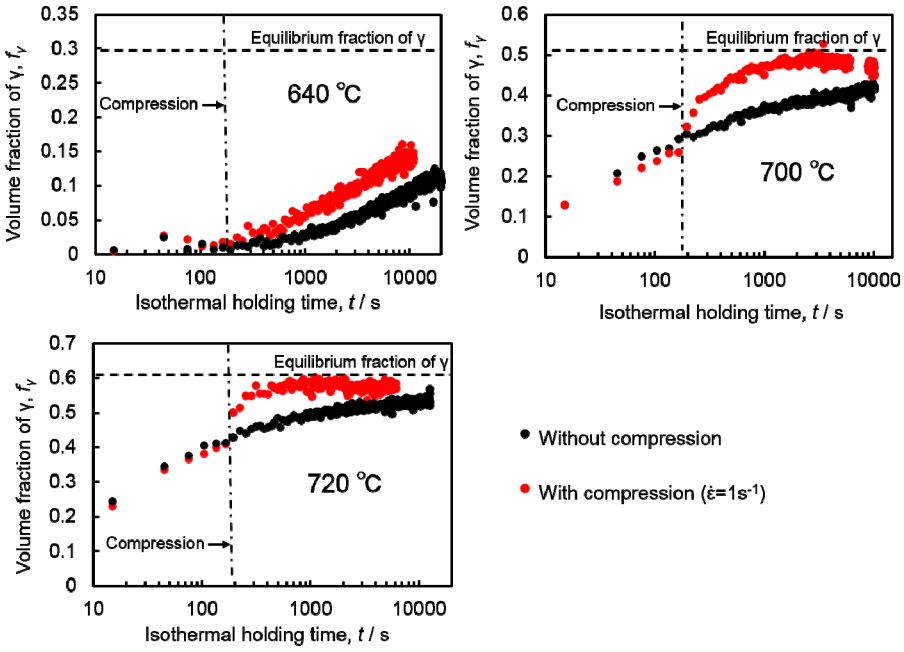


**Figure 12** Volume fractions of reversely transformed austenite at 640°C, 700°C, and 720°C (black plots: without deformation, red plots: with compressive deformation at a strain rate of 1 $s^{-1}$).

2. 実験方法及び結果（つづき） Experimental method and results (continued)

**(2-2) Dynamic ferrite transformation behavior during thermomechanical processing**

Dynamic ferrite transformation is a ferrite transformation occurring during deformation of austenite. Nowadays, thermomechanical controlling process utilizing dynamic ferrite transformation has been received much attention because an ultrafine-grained ferrite structure with grain size less than 1 μm can be achieved. So far, however, many aspects of dynamic ferrite transformation, such as deformation condition for the occurrence of dynamic ferrite transformation, formation mechanism of the ultrafine-grained structure, partitioning behavior of elements, etc., have not been fully understood yet.

In the present experiment, changes in lattice parameters of ferrite and austenite during dynamic ferrite transformation were quantitatively measured by *in-situ* neutron diffraction using the newly developed thermomechanical processing simulator. **Figure 13** presents the change in lattice constant of ferrite in the Fe-2Mn-0.4C (red, present experiment) and the Fe-2Mn-0.1C (blue, the data were obtained in the former experiment of 2015E0001) at 650 °C. In both of the alloys, the lattice constants of statically transformed ferrite (triangles) do not change during transformation, while those of dynamically transformed ferrite (circles) decreases during transformation. We have also confirmed the same tendency in the dynamic ferrite transformation of the Fe-10Ni-0.1C alloy. It should be noted that the decrease in lattice constant of dynamically transformed ferrite is opposite tendency from the elastic strain by compressive deformation (**Figure 10**). The results suggest that partitioning behavior of elements in dynamic transformation changes with proceeding the transformation, i.e., para-equilibrium partitioning to ortho-equilibrium partitioning.

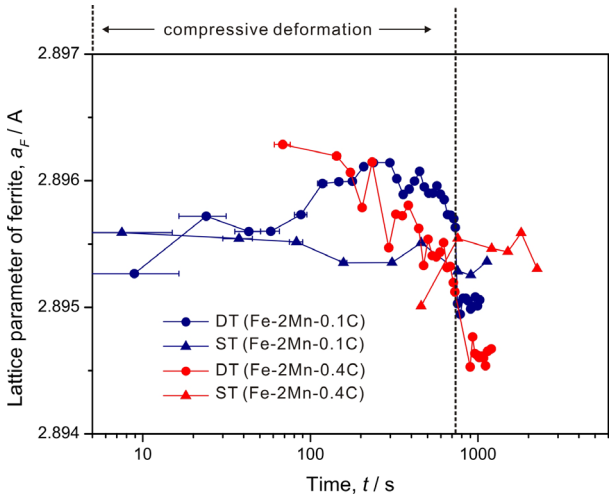


**Figure 13** Change in lattice constants of statically transformed ferrite (triangles) and dynamically transformed ferrite (circles) during transformation in Fe-2Mn-0.4C and Fe-2Mn-0.1C (strain rate: $10^{-3}$ $s^{-1}$).

**(2-3) Transformation behavior of Ti-6Al-4V alloy during thermomechanical processing**

Due to the excellent strength to weight ratio, titanium alloys have been practically used for structural applications. Among several titanium alloys, a Ti-6Al-4V alloy is the most widely used for aerospace, automobile, etc. In general, a Ti-6Al-4V alloy consists of α (hcp) and β (bcc) phases, and morphology and distribution of α and β phases change greatly by thermomechanical processing. It is very important to clarify the effect of transformation temperature and deformation on evolution of α + β dual phase microstructure in the Ti-6Al-4V alloy.

In the present experiment, the transformation behaviors of Ti-6Al-4V alloy were studied by *in-situ* neutron diffraction using the newly developed thermomechanical processing simulator. We have confirmed that no dynamic phase transformation (either α → β or β → α) occurred during the hot deformation. We are now analyzing the obtained data in more detail.